Numerical study on vortex-induced vibrations of a flexible cylinder subjected to multi-directional flows

Yang Qu
Beijing University of Technology
Piguang Wang (wangpiguang1985@126.com)
Beijing University of Technology
Shixiao Fu
Shanghai Jiaotong University: Shanghai Jiao Tong University
Mi Zhao
Beijing University of Technology

Research Article

Keywords: Vortex-induced vibration, Flexible cylinder, Multi-directional flow, Wake oscillator, Fluid-structure interaction

Posted Date: February 15th, 2022

DOI: https://doi.org/10.21203/rs.3.rs-1325741/v1

Noname manuscript No.
(will be inserted by the editor)

Numerical study on vortex-induced vibrations of a flexible cylinder subjected to multi-directional flows

Yang Qu · Piguang Wang · Shixiao Fu · Mi Zhao

Received: date / Accepted: date

Abstract Vortex-induced Vibrations (VIVs) of a flexible cylinder subjected to multi-directional flows have been studied based on a wake oscillator model. The multi-directional flow comprises two slab of flows in different directions, with each slabs having uniform unidirectional profile. The dynamics of the flexible cylinder is described based on the linear Euler-Bernoulli beam theory and a wake oscillator model is uniformly distributed along the cylinder to model the hydrodynamic force acting on it. The dynamics of the coupled system has been solved numerically using the finite element method and simulations have been conducted with the cylinder subjected to multi-directional flows with different angles between the two slabs. A large number of different initial conditions have been applied and more than one steady state responses have been captured for each flow condition. The steady state responses exhibit two different patterns, one is characterized by two waves travelling in the opposite directions, while the other is dominated by a single travelling wave. It has been found that the cross-flow VIV primarily occurs in the local cross-flow direction and a transition of its vibrating direction happens at the interface of the two flows. Such transition is not observed in the inline VIV and significant vibrations at the double frequency appear in both local cross-flow and inline directions. Energy analysis shows that this transition is boosted by a specific energy transfer pattern between the structure and the flow, which excites the vibration of the cylinder in some directions while damps it in others. It has also been found that this energy transfer is related to certain motion trajectories.

Keywords Vortex-induced vibration · Flexible cylinder · Multi-directional flow · Wake oscillator · Fluid-structure interaction

Y. Qu, P. Wang (Corresponding author) and M. Zhao
Key Laboratory of Urban Security and Disaster Engineering of Ministry of Education, Beijing University of Technology, Beijing 100124, China
E-mail: wangpiguang1985@126.com

Y. Qu and S. Fu
State Key Laboratory of Ocean Engineering, Shanghai Jiao Tong University, Shanghai, 200240, China

1 Introduction

When a circular cylinder is placed in flow, vortices are shed in its wake [18], generating fluctuating hydrodynamic forces in both cross-flow and inline directions. For a fixed cylinder, the frequency of the vortex shedding increases linearly with the flow velocity following the Strouhal law [2]. If the cylinder is free to oscillate, then vibrations will occur to the cylinder. As the shedding frequency approaches the natural frequency of the structure, the vibration gets amplified and the vortex shedding frequency would deviate from the Strouhal law and lock on to the frequency of vibration, leading to significant vibrations over a wide range of flow velocities. These vibrations are called Vortex-induced vibrations(VIVs).

VIV is a well known phenomenon with self-excitation and self-limitation and it occurs to a wide range of slender structures such as chimneys, cables of suspended bridges, suspended power lines, offshore risers and mooring cables, that are subjected to air or water flows [12, 10, 8]. Particularly, in offshore engineering, VIV is one of the main factors that limit the fatigue life of flexible risers and therefore is the focus of extensive recent studies [5, 38, 16, 36]. The majority of studies on VIV have been

on a rigid cylinder with elastic support, either only free to move in one direction (cross-flow/inline) or a coupled motion in both directions is considered. The vibration of an elastically supported rigid cylinder provides the simplest form of VIV from which main features of VIV have been discovered and well understood. For more details on VIVs of rigid cylinders, the readers are referred to [25,32].

Compared to a rigid cylinder, the flow around a flexible one is no longer two dimensional and the spatial variation in the dynamic behaviour of the structure as well as the spanwise change in the vortex shedding pattern make it considerably more difficult to obtain a good understanding on the VIV of a flexible cylinder. Efforts have been made to investigate VIVs of flexible cylinders through experiments with well controlled flow profiles, i.e. uniform or linearly sheared flows [29, 26,27,9,34]. It has been found that the VIV of a flexible cylinder is still mainly characterized by the lock-in phenomenon. However, different from a rigid cylinder which possesses only one natural frequency and therefore lock-in only occurs at one frequency, the VIV of a flexible cylinder would lock onto different natural frequencies of the structure at different locations and time instances, showing patterns of space and time sharing [14]. Besides the difference in lock-in, some other unique characteristics of the VIV for a flexible cylinder, such as multiple frequencies, travelling wave and dual resonance, have also been discovered from experiments. For more details on VIVs of flexible cylinders, the readers are referred to [33,17].

Although VIVs of flexible cylinder have been experimentally studied, they are confined to simple flow profiles, i.e. uniform and linearly sheared flows, due to the limitations of current experimental techniques. However, in practice, the structure is usually subjected to a flow that is neither uniform or linearly sheared [28]. This is particularly the case in ocean where the profile of a current normally varies along the depth, not only in the magnitude of flow velocity but also in the direction of it, yielding substantial differences in the response of a structure compared to that in uniform or linearly sheared flows. There is still a lack of understanding on VIVs of flexible cylinders subjected to complex flow profiles. Especially, to authors' best knowledge, there is little research considers a flow profile with varying directions [13]. The dynamic characteristics of a flexible cylinder subjected to flows with varying directions along the span, namely multi-directional flows, are still unclear.

For VIVs of flexible cylinders subjected complex flow profiles, the numerical simulation is probably the only feasible approach, as it is difficult to generate such flow profiles in a controllable manner with currently available experimental techniques. Computational Fluid Dynamics (CFD) is considered as the best numerical method for solving the fluid-structure interaction problem and it has been applied to simulate VIVs of both rigid and flexible cylinders [4,1,11,37]. Particularly, in [3] simulations have been conducted on the VIV of a flexible cylinder where an exponential flow profile is considered. However, the low efficiency of the CFD approach as well as the demanding for large storage and high computation capability makes it still not a favourable approach for VIV analysis, especially when a large number of simulations is required.

Considering the inherent disadvantages of the CFD approach, reduced-order model has been proposed for the simulation of VIV. A well known model of such type is the wake oscillator model. The fundamental concept of the wake oscillator model is to ignore the complex flow field and simplify the dynamics of the wake, as well as the fluctuating force arising from it, as a nonlinear oscillator. The nonlinear oscillator should contain a limit cycle such that the self-excitation and self-limitation features of VIV can be satisfied. The self-exciting fluctuating force generated by the nonlinear oscillator would excite the structure to vibrate and the resultant structural motion in turn interacts with the wake oscillator through a forcing term, forming a coupled system. Despite of its simple form, the wake oscillator model has been shown to be able to reproduce the main features of VIV for both rigid and flexible cylinders [6,30,19,35,20,7]. The model has also been adopted to analyse fundamental characteristics of VIVs that occur to different marine slender structures [31,22].

In this paper, simulations of VIVs have been conduced for a flexible cylinder subjected to multi-directional flows using the wake oscillator model proposed in [24]. The multi-directional flow consists of two flow slabs over each half of the cylinder. Each flow slab has uniform uni-directional profile and a angle α between the two slabs that varies from $\alpha = 15^\circ$ (almost parallel) to $\alpha = 90^\circ$ (perpendicular to each other) is considered. The steady state responses of the flexible cylinder have been investigated in order to reveal the main dynamic characteristics of VIVs in multi-directional flow conditions.

2 Model description

In this paper, we consider a tensioned flexible cylinder with the properties presented in Table 1. This is the same structure as used in the experiments undertaken by Shell Oil company in the MARINTECK Offshore Basin Laboratory [15]. The configuration of the

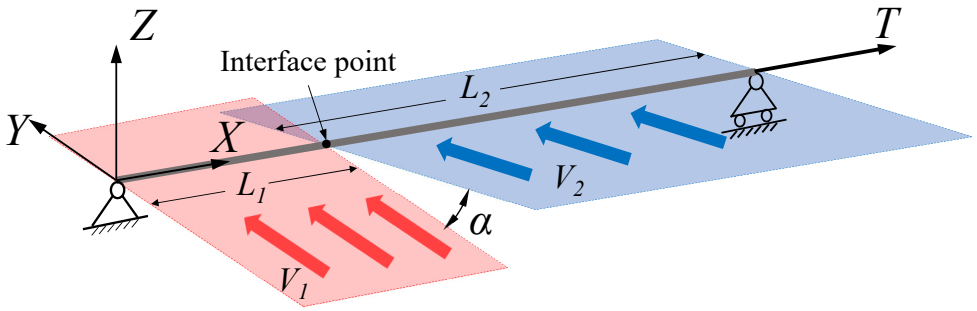

Fig. 1: Configuration of the flexible cylinder and coordinate system

Table 1: Properties of the flexible cylinder

Parameters	Values	Dimension
External diameter	0.03	m
Length	38	m
Aspect ratio	1266	-
Bending Stiffness	572.3	Nm^2
Axial Stiffness	7.82×10^6	N
Mass	1.088	kg/m
Mass ratio	1.54	-

cylinder is illustrated in Fig. 1 together with the multi-directional flow.

The cylinder is subjected to a tension of 6 kN, and according to the Euler-Bernoulli beam theory the displacements of the cylinder Y and Z are governed by equations

$$(m_0 + m_a)\frac{\partial^2 Y}{\partial t^2} + EI\frac{\partial^4 Y}{\partial X^4} - T\frac{\partial^2 Y}{\partial X^2} = F_Y \tag{1}$$

$$(m_0 + m_a)\frac{\partial^2 Z}{\partial t^2} + EI\frac{\partial^4 Z}{\partial X^4} - T\frac{\partial^2 Z}{\partial X^2} = F_Z \tag{2}$$

where m_0 is the mass per unit length of the cylinder, m_a is the potential added mass and T is the tension. The potential added mass is defined as $m_a = \rho\pi D^2 C_a/4$ where ρ is the fluid density, D is the outer diameter of the cylinder and $C_a = 1$ is the potential added mass coefficient.

The cylinder is subjected to two slabs of flows V_1 and V_2 over segments L_1 and L_2, respectively. The flow V_1 is set to be parallel with the X-Y plane while the flow V_2 attacks the cylinder with an angle of α with respect to the flow V_1. The angle α is defined such that the flow V_2 is parallel with V_1 when $\alpha = 0°$ and perpendicular to it at $\alpha = 90°$.

At each cross-section along the cylinder, the vortex-induced forces are decomposed into a lift force F_{VL}, a drag force F_{VD} and an oscillatory in-line force F_{VI}. The drag force F_{VD} acts in the same direction of relative flow velocity U while the lift force F_{VL} acts in the direction perpendicular to it. The oscillatory in-line force F_{VI} is in the inline direction, i.e. the direction of undisturbed flow V. The definitions of the relative flow velocity and the direction of each force are illustrated in Fig. 2. As can be seen from Fig. 2a, the relative flow velocity U is defined as

$$U = \sqrt{U_Y^2 + U_Z^2} \tag{3}$$

where $U_Y = V_Y - \frac{\partial Y}{\partial t}$ and $U_Z = V_Z - \frac{\partial Z}{\partial t}$. The components of undisturbed flow velocity V in Y and Z directions can be obtained as $V_Y = V\sin\alpha$ and $V_Z = V\cos\alpha$. β represents the angle between the relative flow velocity and Y axis, and it is given by

$$\sin\beta = \frac{U_Z}{U} \tag{4}$$

and

$$\cos\beta = \frac{U_Y}{U} \tag{5}$$

The lift force, drag force and oscillatory in-line force are defined as

$$F_{VL} = \frac{1}{2}C_{VL}\rho D U^2 \tag{6}$$

$$F_{VD} = \frac{1}{2}C_{VD}\rho D U^2 \tag{7}$$

$$F_{VI} = \frac{1}{2}\lambda C_{VL}^2 \rho D\,|U_V|\,U_V \tag{8}$$

where C_{VL} and C_{VD} are lift and drag force coefficients, λ is a empirical parameter and U_V is the relative flow velocity in the in-line direction which can be obtained as

$$U_V = V - \left(\frac{\partial Z}{\partial t}\sin\alpha + \frac{\partial Y}{\partial t}\cos\alpha\right) \tag{9}$$

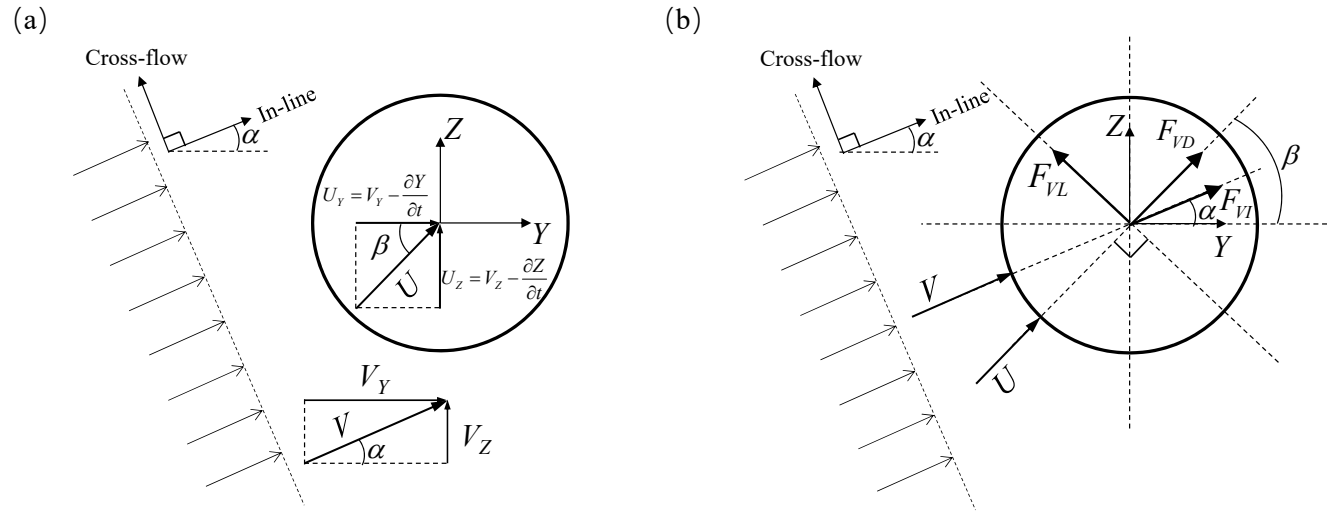

Fig. 2: Illustration of (a) relative flow velocity and (b) force decomposition

The total hydrodynamic forces in Y and Z directions can then be obtained as

$$F_Y = -F_{VL}\sin\beta + F_{VD}\cos\beta + F_{VI}\cos\alpha \tag{10}$$

and

$$F_Z = F_{VL}\cos\beta + F_{VD}\sin\beta + F_{VI}\sin\alpha \tag{11}$$

The drag force coefficient C_{VD} is assumed to be constant, while the dynamic forces caused by vortices are introduced through a time-dependent lift coefficient C_{VL}. The lift coefficient is associated with a wake variable q as $C_{VL} = \frac{q}{2}C_{L0}$ where C_{L0} is the lift force coefficient measured on a fixed cylinder. The dynamics of q is described by a van der Pol type non-linear oscillator which is given as

$$\frac{\partial^2 q}{\partial t^2} + \epsilon\omega_s(q^2-1)\frac{\partial q}{dt} + \omega_s^2 q - \kappa\frac{\omega_s^4 D\frac{\partial \Gamma^2}{\partial t^2}}{\omega_s^4 D^2 + \left(\frac{\partial \Gamma^2}{\partial t^2}\right)^2}q = \frac{A}{D}\frac{\partial \Lambda^2}{\partial t^2} \tag{12}$$

where ϵ, κ and A are tuning parameters, $\omega_s = 2\pi V\mathrm{St}/D$ is the Strouhal freqency and St is the Strouhal number, Γ and Λ represent in-line and cross-flow displacements, which can be obtained as

$$\Gamma = Y\cos\alpha + Z\sin\alpha \tag{13}$$

and

$$\Lambda = Y\sin\alpha + Z\cos\alpha \tag{14}$$

The hydrodynamic force model presented here is referred as wake oscillator model. Instead of modelling the flow field, the wake oscillator model uses a non-linear oscillator, which is coupled with the motion of structure, to described the dynamic vortex shedding process or the hydrodynamic force associated to it. The van der Pol type equation is the most commonly adopted non-linear oscillator. In its early development, the wake oscillator model only considers the cross-flow vibration and the VIV in the in-line direction has been neglected. However, in practical application, the VIV normally occurs simultaneously in both cross-flow and in-line directions in a coupled manner. The specific model that we have used here is the one proposed recently in [24]. This new model, compared to the conventional wake oscillator model, contains two important improvements. Firstly, in addition to the coupling with the cross-flow motion (right hand side of the Eq. (12)), an in-line coupling term (the fourth term on the left hand side of Eq. (12)) is introduced. Secondly, an oscillatory force F_{VI} that is coupled to the quadratic of the lift force is introduced in the in-line direction.

The quadratic coupling in Eq. (8) is based on the relation that has been found between the cross-flow and in-line forces for the case of a fixed cylinder [21]. In the case where the current is aligned with Y axis, i.e. $\alpha = 0°$, and structure does not move, i.e. $Y = 0$ and $Z = 0$, the total in-line force is the summation of F_{VD} and F_{VI} as

$$F_{inline} = F_{VD} + F_{VI} = \frac{1}{2}\rho DV^2\left(C_{VD} + \lambda C_{VL}^2\right) \tag{15}$$

which is in the same form as proposed in [21]. If the lift force acting on a fixed cylinder is given as $C_{VL} = C_{L0}\sin(\omega t)$, then substituting it into Eq. (15) and defining the inline force coefficient as $C_{inline} = F_{inline}/\left(\frac{1}{2}\rho DV^2\right)$ result in

$$C_{inline} = C_{VD} + \frac{1}{2}\lambda C_{L0}^2\left(1 - \cos(2\omega t)\right) \tag{16}$$

It is clear from Eq. (16) that the inline force coefficient contains a steady component with magnitude of $C_{VD} + \frac{1}{2}\lambda C_{L0}^2$ and an oscillatory component with amplitude of $\frac{1}{2}\lambda C_{L0}^2$. Comparing the steady and oscillatory components of C_{inline} to those measured on a fixed cylinder, the values of C_{VD} and λ can be determined as

$$C_{VD} = C_D - \frac{1}{2}\lambda C_{L0}^2 \tag{17}$$

and

$$\lambda = 2\frac{C_{D0}}{C_{L0}} \tag{18}$$

where C_D and C_{D0} are the mean and the amplitude of fluctuating drag coefficients of a fixed cylinder. In the present paper, the same empirical and tuning parameters as those given in [23], where the VIV of the same structure is simulated, are adopted, i.e. $C_{L0} = 0.3$, $C_{D0} = 0.1$, $C_D = 1.2$, $\epsilon = 0.08$, $A = 8$, $\kappa = 5$ and $\mathrm{St} = 0.2$.

The wake oscillators (Eq. (12)) are uniformly distributed along the cylinder at each cross-section and are coupled with the local structure motions, leading to a spatial and time varying distribution of wake variable, i.e. $q(x,t)$. The whole coupled system can be solved using finite element method. Both the structure and wake variable are discretized with respect to x using the cubic Hermite shape functions, resulting in three sets of ordinary differential equations

$$\mathbf{M}_s\ddot{\mathbf{e}}_Y + \mathbf{K}_s\mathbf{e}_Y = \mathbf{F}_Y \tag{19}$$

$$\mathbf{M}_s\ddot{\mathbf{e}}_Z + \mathbf{K}_s\mathbf{e}_Z = \mathbf{F}_Z \tag{20}$$

$$\mathbf{M}_q\ddot{\mathbf{q}} + \mathbf{C}_q\dot{\mathbf{q}} + \mathbf{K}_q\mathbf{q} = \mathbf{R} \tag{21}$$

The above ordinary differential equations are solved in the time domain using Newmark-β time integration method.

With flows attacking the cylinder from different directions, the influence of the variation in the flow direction and velocity magnitude on the hydrodynamic force at the interface point of the flows should be taken into account. In practice, the change of the flow direction and velocity cannot be abrupt and a transition zone must present between the flows. In this transition zone, the flow may not be steady and the three dimensional effect could be significant due to the shear forces between the flows. There is so far no hydrodynamic force model applicable to such a flow condition. It is therefore assumed here that no regular vortex shedding process occurs in the transition zone and the hydrodynamic forces acting on the cylinder are simplified as potential inertia and viscous drag forces following the Morison equation. This is, in the model, achieved by enforcing the wake variable $q = 0$ at the interface point of flows

3 Response patterns

Although the model described in previous section can be applied to flow conditions with varying L_1, L_2, V_1 and V_2, the present study focuses on the cases with $L_1 = L_2$ and $V_1 = V_2$. The flow velocity is fixed to be $V_1 = V_2 = 1.5$ m/s. Six flow conditions with different angles between the two flows have been considered, namely $\alpha = 15°$, $30°$, $45°$, $60°$, $75°$ and $90°$. Being a non-linear problem, the VIV of a flexible cylinder may have different steady state responses. To obtain as many response patterns as possible, a large number of simulations have been conducted with different initial conditions. For each simulation, the initial displacement and velocity of the cylinder were set to be zero, the initial value of zero was also taken for the velocity of the wake variable q, while different initial conditions were applied by generating random values for the displacement of wake variable q along the cylinder. In one type of initial condition, uniformly distributed random values in the interval (-2,2) were generated for the displacements of q along the entire span of the cylinder. In another type of initial condition, uniformly distributed random values in the interval (-2,2) were only generated for the wake variables over half span of the cylinder, i.e. the span L_1, while the wake variables over the other half span were set to be zero.

For each flow condition, both types of initial conditions have been applied and ten random initial conditions were generated for each type, resulting 20 simulations for each flow condition and total of 120 simulations for all. To save the computational time, the cylinder was discretized into 60 elements and it has been checked that doubling the number of element does not make significant changes to the simulation results.

For each flow condition, more than one steady state response have been observed in the simulations. In general, all the steady state responses can be categorized into two major types. One type of the response is characterized by two travelling waves that propagate in the opposite directions, while only a single travelling wave is observed in the other type of response. The typical responses of these two types are illustrated in Fig. 3 for the flow condition with $\alpha = 45°$. These two different types of responses will be described in detail in this section.

3.1 Responses with opposing travelling waves

The response pattern that characterized by two opposing travelling waves has been observed in all six flow conditions. Here, one response obtained in the flow condition with $\alpha = 45°$ is taken as an example to illustrate

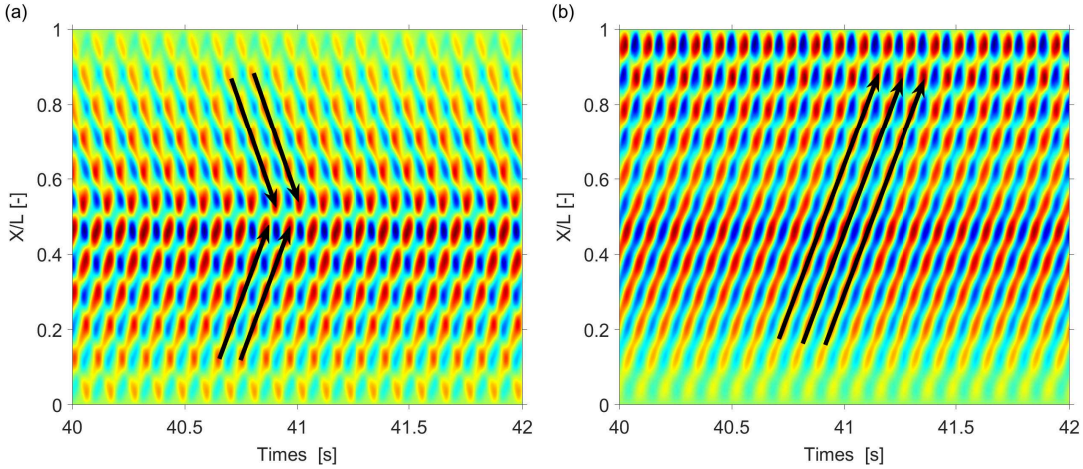

Fig. 3: Different response patterns: (a) two opposing travelling waves; (b) single travelling wave.

such response pattern. Fourier analysis have been conducted to obtain the spectrum of the response and the results are presented in Fig. 4. In Fig. 4, the amplitude of the displacement is normlized by the diameter of the cylinder D and the frequency is normalized by the Strouhal frequency. It can be seen from Fig. 4 that the response of the cylinder is dominated by two frequency components, one is close to but slightly lower than the Strouhal frequency (1X) and the other has the doubled value (2X). These two frequency components have been detected in all simulations and were found to dominate the cylinder response. The vibration at the frequency 1X is a result of cross-flow VIV while that at the frequency 2X is due to the inline VIV. It needs to emphasized here that since the cylinder is subjected to flows with different directions, although the 1X frequency component is fundamentally caused by the cross-flow VIV, it does not necessarily only appear in the local cross-flow direction. The same applies to the inline VIV at the frequency 2X. It is therefore important to identify the dominant vibrating direction of each frequency component. Here, the dominant vibrating direction is defined as the direction with maximum vibration amplitude.

To obtain the dominant vibrating direction, the vibrations of the cylinder in Y and Z directions are firstly projected to other directions as

$$W_\theta(x) = Y\cos\theta + Z\sin\theta \tag{22}$$

where θ is the angle between the Y axis and the direction to be projected, $\theta = 0°$ corresponds to the Y direction and $\theta = 90°$ corresponds to the Z direction. The θ is varied from 0° to 180° to generate vibrations in all directions. Applying Fourier analysis to W_θ, the amplitude spectra can be obtained, from which the amplitudes of W_θ in all directions can be extracted at both 1X and 2X frequencies, see Fig. 5. The dominant vibrating direction at one location is determined by finding the maximum amplitude of W_θ, indicated by the black lines in Fig. 5.

It can be seen from Fig. 5a that the dominant vibrating direction of the cross-flow VIV is generally in agreement with the local cross-flow direction, except that around the interface of the two flows. The dominant vibrating direction of the inline VIV, on the other hand, oscillates significantly around the local inline direction, as can be seen from Fig. 5b.

To better illustrate the characteristics of this response pattern and reveal the underlying mechanism causing it, the total response of the cylinder was decomposed into two travelling waves, one with orientation from $X/L = 0$ to $X/L = 1$ and the other in the opposite direction. Hilbert transform is a well developed approach for such decomposition. Assuming the total response of the cylinder is described mathematically in the form of complex as $W(x)\,e^{\mathrm{i}\omega t}$ where $W(x)$ is a position-dependent complex value representing the change in the phase and amplitude of cylinder vibration. The $W(x)$ can be further expressed as two travelling waves in opposite propagating directions as

$$W(x) = W_+(x)\,e^{\mathrm{i}kx} + W_-(x)\,e^{-\mathrm{i}kx} \tag{23}$$

where k is the wave number, W_+ (being complex) represents the amplitude and phase of the wave propagating in a positive (+x) direction and W_- is the counter part of W_+ travelling in the negative direction (-x). Applying Hilbert transform to $W(x)$ results in

$$\mathbf{H}[W(x)] = -\mathrm{i}W_+(x)\,e^{\mathrm{i}kx} + \mathrm{i}W_-(x)\,e^{-\mathrm{i}kx} \tag{24}$$

Then, it can be obtained from Eqs. (23) and (24) that

$$W_\pm(x)\,e^{\pm\mathrm{i}kx} = -\frac{1}{2}\mathrm{i}\left(\mathrm{i}W(x) \mp \mathbf{H}[W(x)]\right) \tag{25}$$

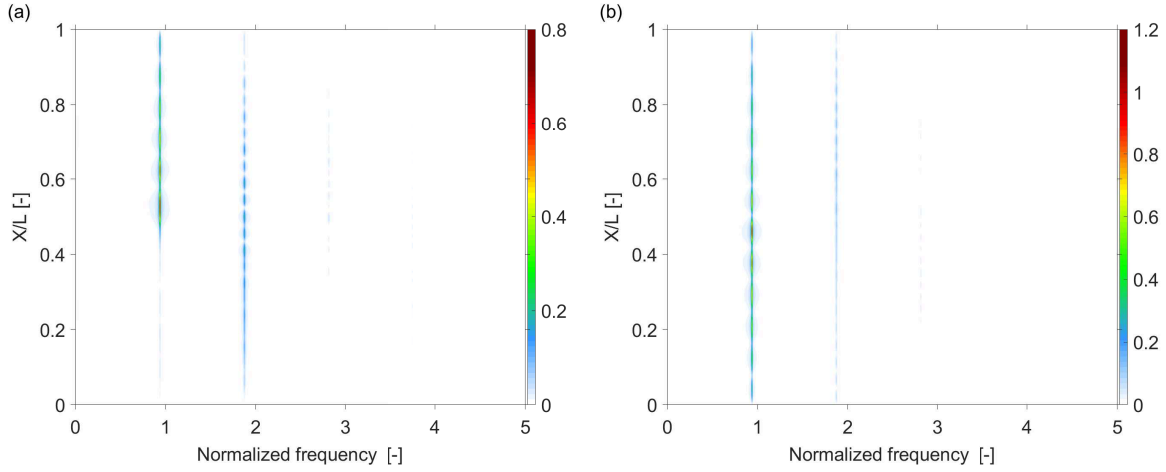

Fig. 4: Amplitude spectra of displacement along the cylinder in (a) Y and (b) Z directions for one response in the flow condition with $\alpha = 45°$.

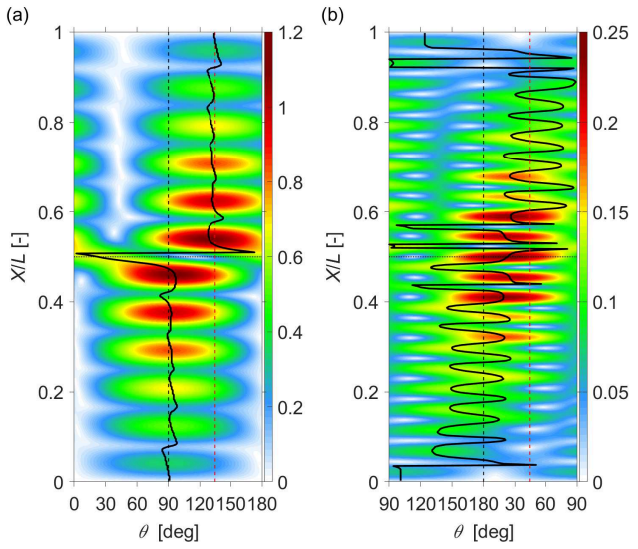

Fig. 5: Spanwise evolutions of cylinder displacement amplitudes W_θ at (a) 1X and (b) 2X frequencies for one response in the flow condition with $\alpha = 45°$. The thick black line is the trace of maximum amplitudes along the cylinder. The horizontal dotted line represents the interface between the two flows; vertical black dashed line represents the local cross-flow/inline direction of flow V_1 and vertical red dashed line represents the cross-flow/inline direction of flow V_2.

from which the amplitudes and phases of the two waves can be extracted.

Applying the wave decomposition method described above, the two travelling waves have been obtained in all vibrating directions θ and their amplitudes are presented in Fig. 6. The dominant vibrating direction of the wave at each location along the cylinder can then be identified by finding the maximum amplitude, as indicated by the black lines in Fig. 6. The two opposing travelling waves characteristic of the response can be clearly identified from Fig. 6. VIVs have been excited by both flows and progress toward each other, being damped as they propagating in the zone of the other flow. For the cross-flow VIV, its dominant vibrating direction quickly changes to comply with the local cross-flow direction after it encounters the other flow, as can be seen from Figs. 6a,b. Different from the cross-flow VIV, the dominant vibrating direction of the inline VIV continuously deviates away from the local inline direction instead of trying to comply with it, as can be seen from Fig. 6c,d.

The amplitudes and phases of the travelling waves in their dominant vibrating direction have been extracted following the black lines in Fig. 6 and the results for the cross-flow VIV are presented in Fig. 7. For better comparison, the results for the wave travelling in the direction from $X/L = 1$ to $X/L = 1$ are plotted up side down. It can be seen that the two waves are identical with respect to the amplitude (Fig. 7a), but have a phase difference of π (Fig. 7b). This results in a symmetrical response pattern and a local minimum displacement amplitude at the mid-span point of the cylinder.

Symmetrical response has been found in all flow conditions, but it is not always corresponds to a phase difference of π. In some simulations with symmetrical responses, the phase difference between the two waves is 0 which causes a peak displacement amplitude at the interface point.

Besides the symmetrical response, asymmetrical responses have also been observed in simulations. For the asymmetrical response with two opposing travel-

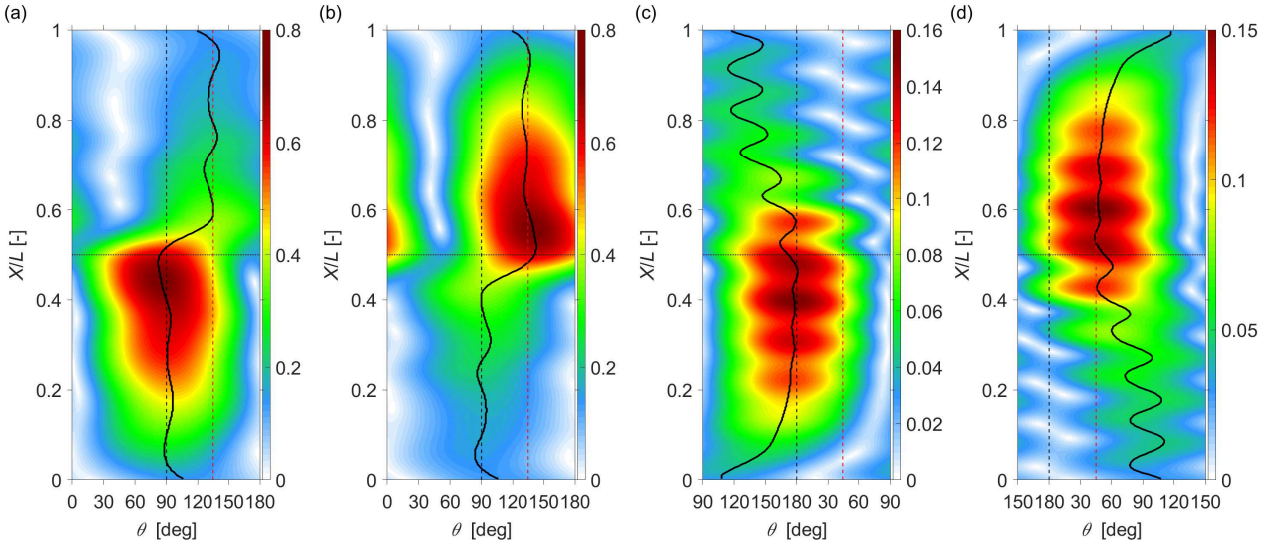

Fig. 6: Amplitudes of decomposed travelling waves with propagating directions (a,c) from $X/L = 0$ to $X/L = 1$ and (b,d) from $X/L = 1$ to $X/L = 0$ at frequencies (a,b) 1X and (c,d) 2X for one response in the flow condition with $\alpha = 45°$. The thick black line is the trace of maximum amplitude along the cylinder. The horizontal dotted line represents the interface between two flows; vertical black dashed line represents the cross-flow/inline direction of flow V1 and vertical red dashed line represents the cross-flow/inline direction of flow V2.

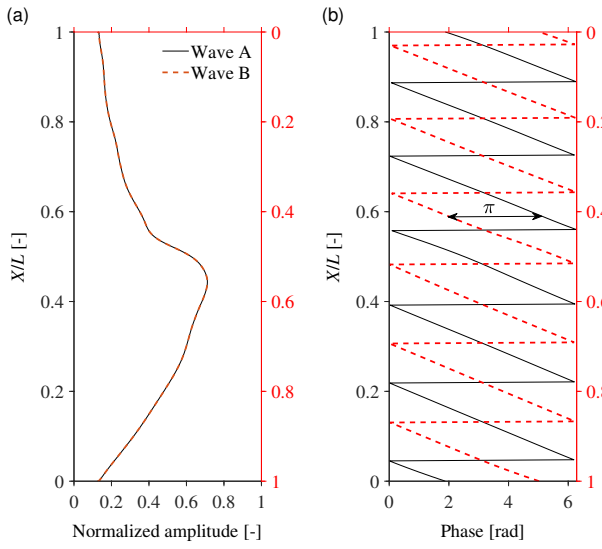

Fig. 7: Spanwise evolutions of (a) amplitudes and (b) phases of decomposed travelling waves in the dominant vibrating directions at frequency 1X for one response in the flow condition with $\alpha = 45°$. Wave A represents the wave with propagating direction from $X/L = 0$ to $X/L = 1$ and Wave B represents the wave in the opposite direction.

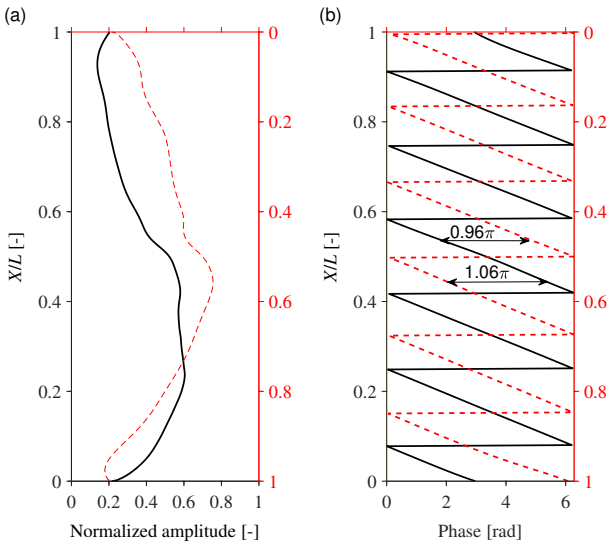

Fig. 8: Spanwise evolutions of (a) amplitudes and (b) phases of decomposed travelling waves in the dominant vibrating directions at frequency 1X for an asymmetrical response in the flow condition with $\alpha = 30°$.

ling waves, it is expected that the two waves neither are identical in amplitude nor have a phase difference of π or 0. The amplitudes and phases of the travelling waves decomposed from the cross-flow VIV of one asymmetrical response in the flow condition with $\alpha = 30°$ are presented in Fig. 8 as an example.

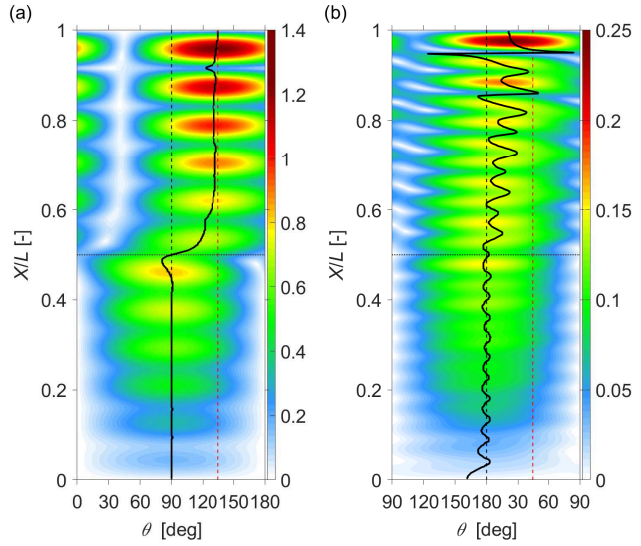

Fig. 9: Spanwise evolutions of cylinder displacement amplitudes at (a) 1X and (b) 2X frequencies for a response with single travelling wave in the flow condition with $\alpha = 45°$. The thick black line is the trace of maximum amplitude along the cylinder. The horizontal dotted line represents the interface between two flows; vertical black dashed line represents the cross-flow/inline direction of flow V1 and vertical red dashed line represents the cross-flow/inline direction of flow V2.

3.2 Responses with single travelling wave

This type of response is characterized by a single travelling wave vibrating in different directions but with the same propagating direction and is only observed in simulations with random initial conditions for the flow conditions with $\alpha = 15°$ and $45°$. However, it was found that such response pattern can also be captured in other flow conditions, if a specific initial condition in the form of a travelling wave is applied to the displacement and velocity of the cylinder.

The amplitudes of the cylinder displacements in all directions at 1X and 2X frequencies are presented in Fig. 9 for a response with single travelling wave, where the dominant vibrating direction of the wave along the cylinder is indicated by the thick black line. For the cross-flow VIV, the dominant vibrating direction is in a generally good agreement with the local cross-flow direction over most span of the cylinder, as can be seen from Fig. 9a. A transition of the dominant vibrating direction occurs close to the interface point. The dominant vibrating direction of the inline VIV is in agreement with the local inline direction over the first half span of the cylinder, i.e. where the VIV originates, but is significantly different from the local inline direction over the other half span.

The amplitudes of decomposed travelling waves for this response are presented in Fig. 10. It is clear from Fig. 10 that the response of the cylinder is dominated by a single travelling wave progressing in the direction from $X/L = 0$ to $X/L = 1$ for both cross-flow and inline VIVs. The travelling wave in the opposite propagating direction is only observed close to the end of the cylinder as a result of reflection. This implies that the VIVs have been excited by flow V_1 and travel towards flow V_2. However, instead of getting damped by the flow V_2, the magnitude of the wave is continuously amplified during propagation. The dominant vibrating direction of the travelling wave quickly changes to the local cross-flow direction as it enters the flow V_2, see the black line in Fig. 10a. This quick transition is not observed in Fig. 10c for the inline VIV, although the dominant vibrating direction of the wave is seen to gradually vary towards the local inline direction.

3.3 Influence of phase difference

It was found from simulations that there is more than one steady state solution under each flow condition. The number of steady state responses that captured with random initial conditions is summarized in Table 2. For steady state response that characterized by two opposing travelling waves, the phase differences between the waves are also presented in Table 2. Here, the phase difference is determined at the mid-span point of the cylinder, i.e. the interface point between the two flows. If the summation of the phase differences in two responses equals to 2π, then these two responses are actually the same steady state solution. The number in the parentheses after the phase difference represents how many simulations converge to this response.

It can be seen from Table 2 that despite a large number of random initial conditions have been applied, only a few steady state solutions were obtained. Among those solutions with two opposing travelling waves, it is interesting to find that the phase differences between the two waves seem to prefer certain values. Then, the question arises as is this a coincidence or the VIV in such flow condition has a preference on the phase difference? To answer this question, simulations have been conducted with initial conditions that have artificially shifted phase differences to check whether new steady state solutions can be detected.

The initial condition with phase shift between the two waves is obtained by combining the responses of the two segments L_1 and L_2 at different time instances. For example, the response of the cylinder segment L_1

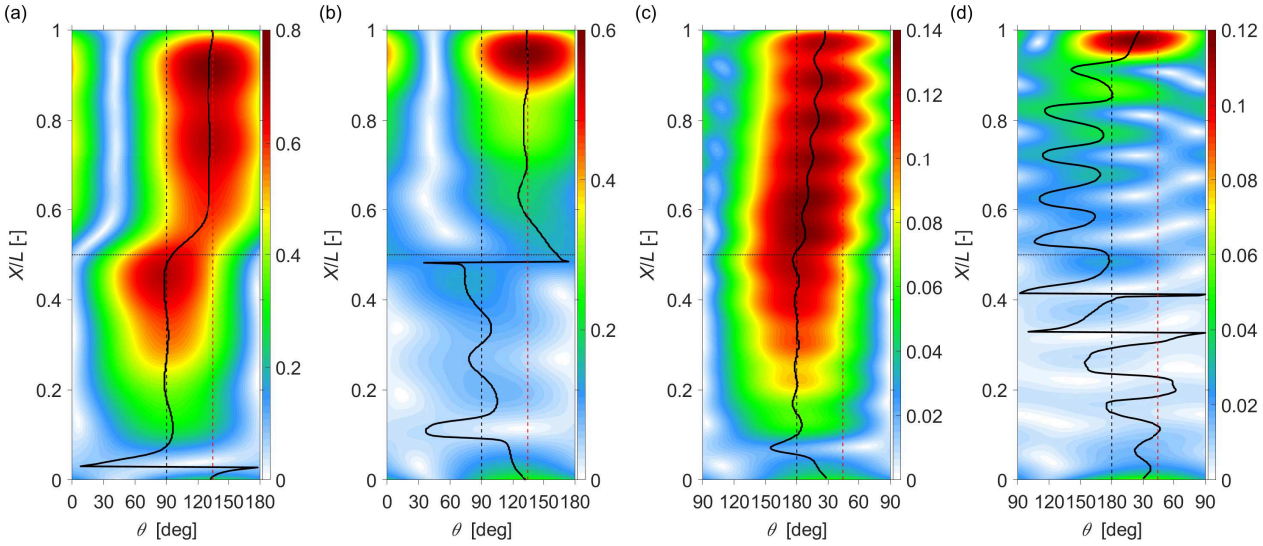

Fig. 10: Amplitudes of decomposed travelling waves with propagating directions (a,c) from $X/L = 0$ to $X/L = 1$ and (b,d) from $X/L = 1$ to $X/L = 0$ at frequencies (a,b) 1X and (c,d) 2X for a response with single travelling wave in the flow condition with $\alpha = 45°$. The thick black line is the trace of maximum amplitude along the cylinder. The horizontal dotted line represents the interface between two flows; vertical black dashed line represents the cross-flow/inline direction of flow V_1 and vertical red dashed line represents the cross-flow/inline direction of flow V_2.

Table 2: Summary of steady state responses and phase differences

Response	15°		30°		45°		60°		75°		90°	
R1	π	(11)	π	(16)	π	(17)	0	(1)	π	(9)	0	(17)
R2	1.96π	(1)	1.06π	(2)	0	(2)	$0.81\pi, 1.19\pi$	(19)	$0.73\pi, 1.27\pi$	(4)	1.37π	(3)
R3	0.99π	(2)	0.98π	(2)	S	(1)	-		$0.94\pi, 1.06\pi$	(7)	-	
R4	$\approx \pi$	(2)	-		-		-		-		-	
R5	S[1]	(3)	-		-		-		-		-	

[1] S means the response is characterized by a single travelling wave instead of two opposing travelling wave.

Table 3: Phase differences of steady state responses obtained with artificial phase shifts

Case	Initial phase difference							
	0	$\frac{1}{7}\pi$	$\frac{2}{7}\pi$	$\frac{3}{7}\pi$	$\frac{4}{7}\pi$	$\frac{5}{7}\pi$	$\frac{6}{7}\pi$	π
15°	0	0	S	S	π	π	π	π
30°	0	0	S	π	π	π	π	π
45°	0	0	π	π	π	π	π	π
60°	0	0	0	0	1.19π	0.81π	1.19π	1.19π
75°	0	0.73π	π	0.73π	0.73π	0.73π	π	π
90°	0	0	1.37π	1.37π	1.37π	1.37π	1.37π	0

at time t is combined with the response of the cylinder segment L_1 at time $t - \delta t$. The resultant phase shift is then approximately $\omega\delta t$. Using this method, simulations have been conducted using initial conditions with phase differences varying from 0 to π. The final phase differences between the two travelling waves of the obtained steady state responses are calculated and the results are presented in Table. 3. It can be seen from Table. 3 that, although a phase shift have been introduced in the initial condition, the phase difference in the steady state response still converges to either 0 or π under flow conditions with $\alpha = 15°$, 30° and 45°. For larger angles of $\alpha = 60°$, 75° and 90°, asymmetrical responses with phase differences other than 0 and π were also obtained. It needs to emphasized that the responses obtained in the simulations with phases shifts

do not cover all the responses for the flow conditions with $\alpha = 15°$ and $30°$, as some other asymmetrical responses under these two flow conditions have been captured with random initial conditions. On the other hand, the responses shown in Table 3 for the flow conditions with $\alpha = 45°$, $60°$, $75°$ and $90°$ are the same as those obtained with random initial conditions. Particularly, no response with phase difference π has been captured under flow conditions $\alpha = 60°$ and $90°$.

As shown in Table 3, no other steady response was obtained by varying the initial phase difference between the two waves. The VIV of the cylinder tend to converge to a few steady state solutions and these solutions have certain phase differences with varying α. This implies that, for the flow conditions considered in the present paper, the VIVs characterized by two opposing travelling waves indeed have a preference on the phase difference and this preference changes with α.

4 Response amplitudes

The amplitudes of the cylinder displacements at the two dominant frequencies 1X and 2X can be extracted from the spectrum analysis and their spanwise evolutions have been obtained for each steady state response. Before extracting these informations, the displacements were firstly projected to local cross-flow and inline directions according to Eqs. (13) and (14). Therefore, the

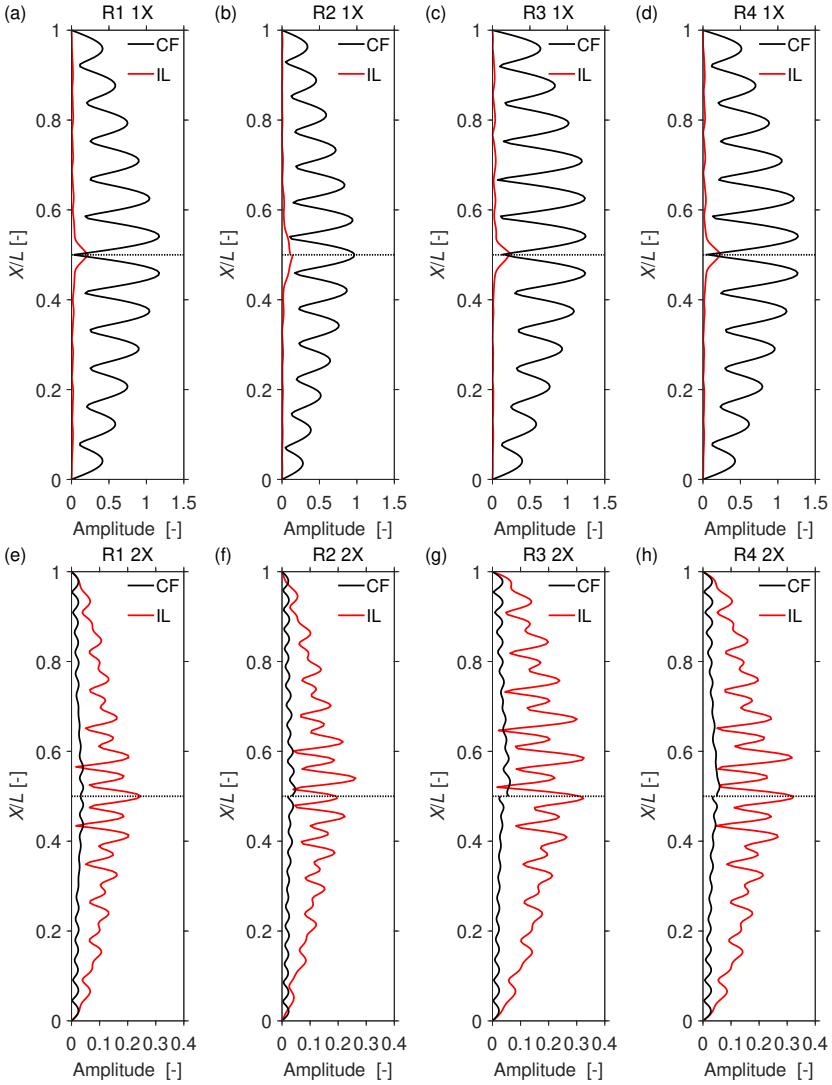

Fig. 11: Normalized amplitudes of displacements at frequencies (a-d) 1X and (e-h) 2X along the cylinder in local cross-flow (CF) and inline (IL) directions for the flow condition with $\alpha = 15°$. Only the responses characterized by two opposing travelling waves are presented. The horizontal dotted line represents the interface between the two flows.

amplitudes that presented in the rest of this section correspond to the vibrations in local cross-flow and inline directions.

4.1 Amplitudes of responses with opposing travelling waves

Fig. 11 presents the amplitudes of cross-flow and inline displacements along the cylinder for the flow condition with $\alpha = 15°$. In general, the cross-flow and inline VIVs of the cylinder are in agreement with the local cross-flow and inline directions. Particularly, the cross-flow VIV appears primarily in the local cross-flow direction and is only observed with very small amplitudes in the local inline direction over a short span of the cylinder around the interface point. The inline VIV, on the other hand, is observed in both local cross-flow and inline directions along the entire cylinder. However, its component in the local inline direction is significantly larger (over ten times at some locations) than that in the local cross-flow direction. This is in agreement with the transition of dominant vibrating direction as discussed in the previous section. It is noted that the responses of R1, R3 and R4 in this flow condition are very close to each other, but still slight differences can be observed either in the inline response (for R1) or in the cross-flow response at locations around $X/L = 0.65$ (for R3).

The amplitudes of cylinder displacements in local cross-flow and inline directions are presented in Fig. 12 for the flow condition with $\alpha = 30°$. Three different responses have been observed from simulations and they are characterized by the same patterns as those of $\alpha = 15°$, and therefore are not described in detail here. Again, two responses, i.e. R1 and R3, with almost exact amplitudes have been captured. Still slight discrepancy between the two responses can be observed in the evolution of displacement around $X/L \approx 0.7$.

For the flow condition with $\alpha = 45°$, only two responses, both exhibit symmetrical patterns, have been observed in the simulations with two opposing waves. The displacement amplitudes of these two responses are presented in Fig. 13. It is clear from Fig. 13 that different wave length have been excited in the two responses. It has been shown in Table 2 that the two waves in R1 have a phase difference of π, while the phase difference between the two waves in R2 is 0. Correspondingly, a local minimum/peak amplitude is observed at the mid-span point of the cylinder.

Amplitudes of local cross-flow and inline displacements for the flow conditions with $\alpha = 60°$, $75°$ and $90°$ are presented in Figs. 14-16. The fundamental characteristics of these responses are similar to those of $\alpha = 15°$, $30°$ and $45°$. For all cases, vibrations at the frequency 1X primarily occur in the local cross-flow direction and are only observed in the local inline direction over a short span close to the interface point. However, the size of this span expands with increasing α and the magnitude of the 1X frequency component in the local inline direction also increases. This is actually expected, since larger angle between the two flows

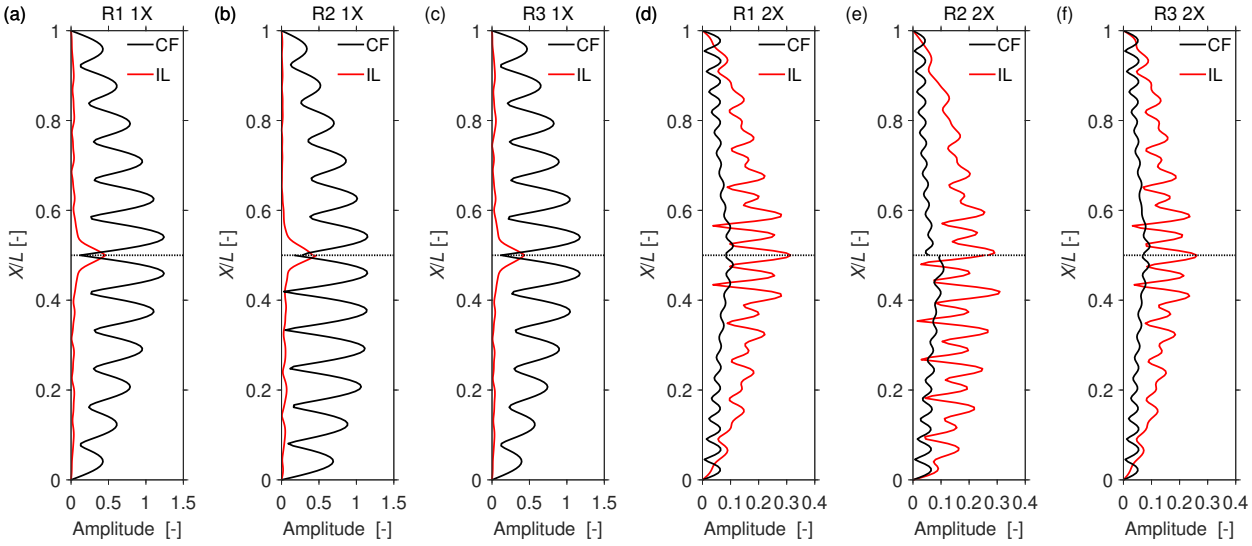

Fig. 12: Normalized amplitudes of displacements at frequencies (a-c) 1X and (d-f) 2X along the cylinder in local cross-flow (CF) and inline (IL) directions for the flow condition with $\alpha = 30°$. Only the responses characterized by two opposing travelling waves are presented. The horizontal dotted line represents the interface between the two flows.

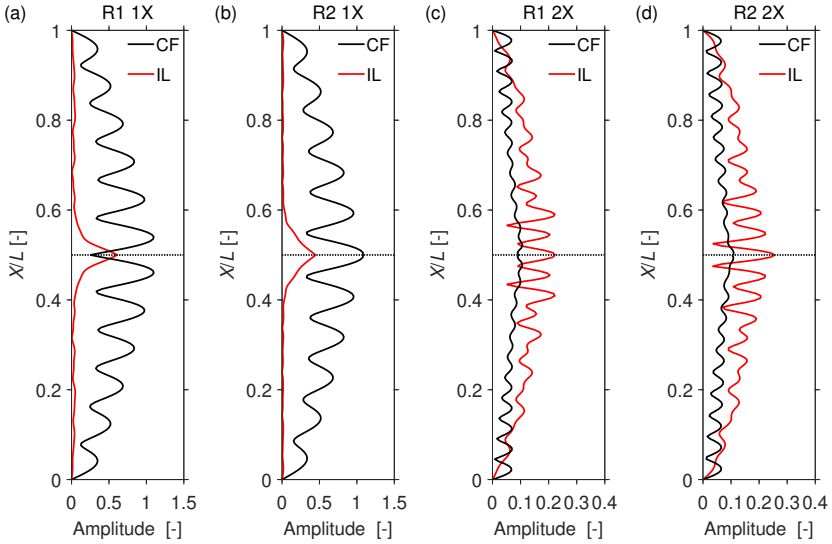

Fig. 13: Normalized amplitudes of displacements at frequencies (a-c) 1X and (d-f) 2X along the cylinder in local cross-flow (CF) and inline (IL) directions for the flow condition with $\alpha = 45°$. Only the responses characterized by two opposing travelling waves are presented. The horizontal dotted line represents the interface between the two flows.

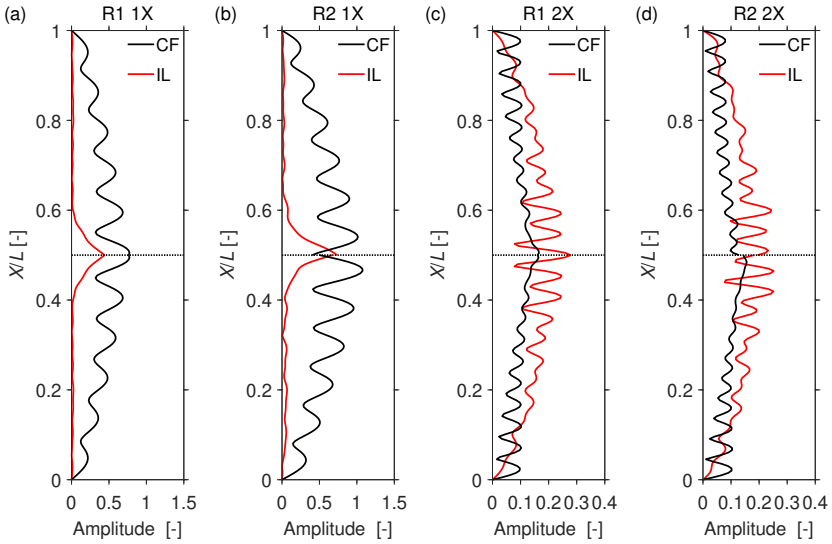

Fig. 14: Normalized amplitudes of displacements at frequencies (a-c) 1X and (d-f) 2X along the cylinder in local cross-flow (CF) and inline (IL) directions for the flow condition with $\alpha = 60°$. Only the responses characterized by two opposing travelling waves are presented. The horizontal dotted line represents the interface between the two flows.

means more contributions from the cross-flow VIV excited by one flow to the vibration in the inline direction of the other flow due to a $\sin\alpha$ relation between the two, as can be seen from Eq. 13. For the vibrations at frequency 2X, they mainly appear in the local inline direction for the cases with small angle α, but become predominant in both directions over the entire span of the cylinder at large angles.

The tendency of variations in the amplitudes of cross-flow and inline displacements can be better seen from Fig. 17 where the maximum amplitudes at frequencies 1X and 2X for all responses are presented. In general, the magnitudes of both cross-flow VIV (black starts in Fig. 17a) and inline VIV (red diamonds in Fig. 17b) decrease with increasing angle.

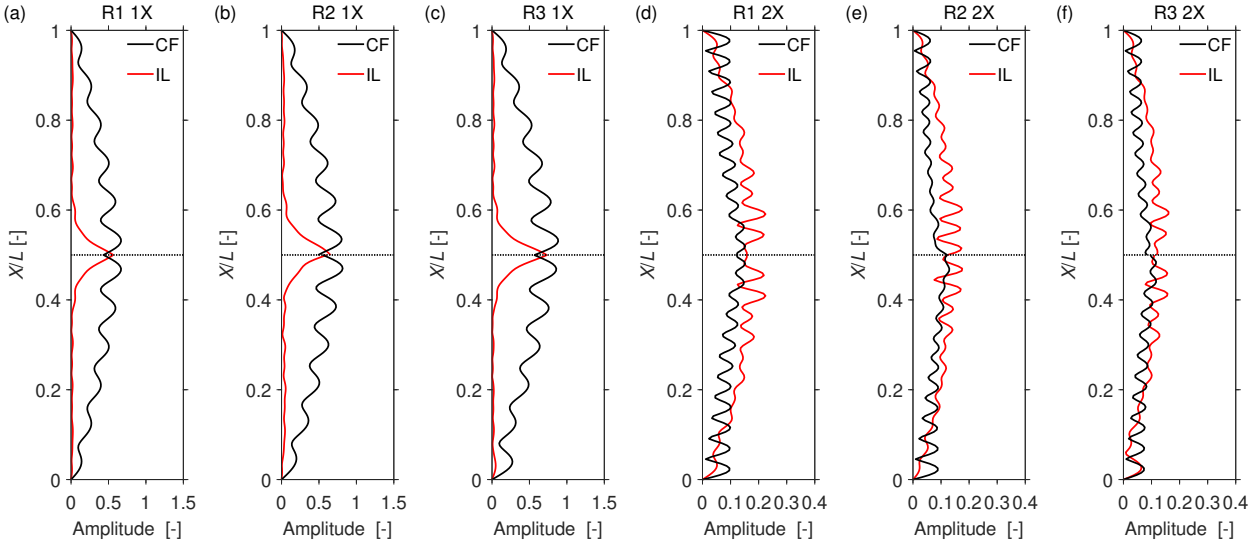

Fig. 15: Normalized amplitudes of displacements at frequencies (a-c) 1X and (d-f) 2X along the cylinder in local cross-flow (CF) and inline (IL) directions for the flow condition with $\alpha = 75°$. Only the responses characterized by two opposing travelling waves are presented. The horizontal dotted line represents the interface between the two flows.

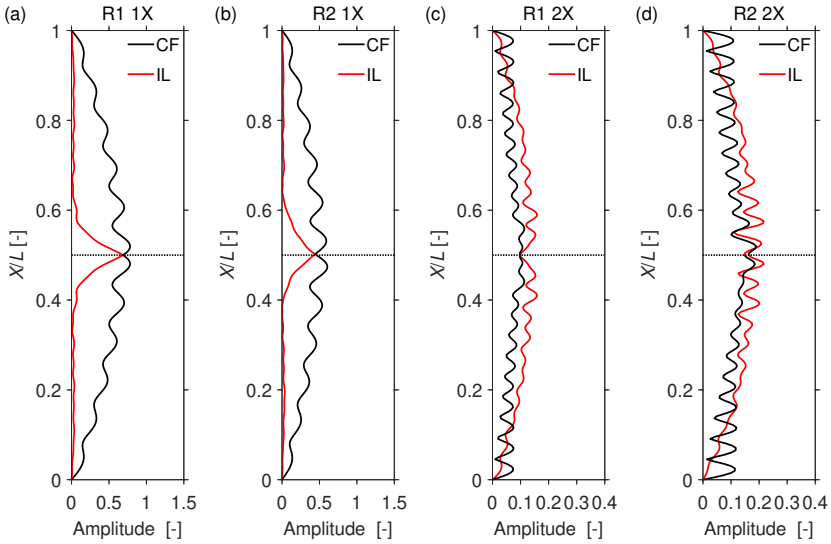

Fig. 16: Normalized amplitudes of displacements at frequencies (a-c) 1X and (d-f) 2X along the cylinder in local cross-flow (CF) and inline (IL) directions for the flow condition with $\alpha = 90°$. Only the responses characterized by two opposing travelling waves are presented. The horizontal dotted line represents the interface between the two flows.

4.2 Amplitudes of responses with single travelling wave

In simulations with random initial conditions, the responses with single travelling wave were only captured in flow conditions with $\alpha = 15°$ and $45°$. However, it was found that if an initial condition in the form of a single travelling is provided, then such type of response can also be obtained in other flow conditions. Therefore, simulations have been re-conducted with modified initial conditions and responses that characterized by a single travelling wave have been successfully captured in all flow conditions. The displacement amplitudes of these responses are presented in Fig. 18

It is clear from Fig. 18 that the responses of the cylinder are dominated by waves travelling in the same

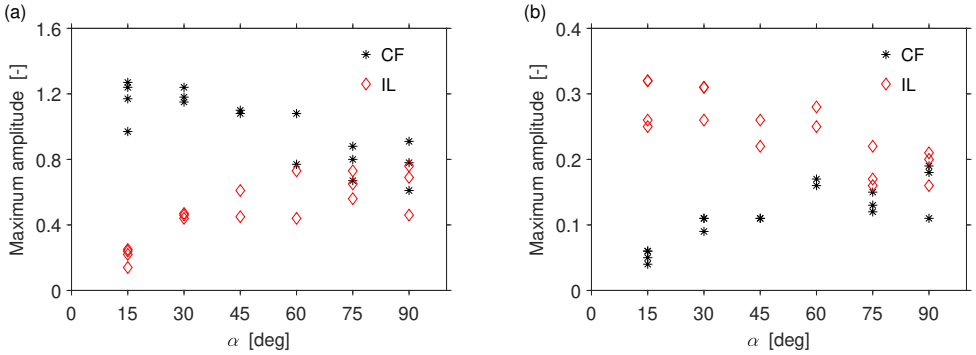

Fig. 17: Maximum amplitudes of normalized cross-flow (CF) and inline (IL) displacements at frequencies (a) 1X and (b) 2X for the responses with opposing travelling waves.

direction. The overall pattern of the amplitude evolution along the span indicates that the vibration has been excited by one flow and then travels towards the other flow. The other flow would take over the wave and the motion at the 1X(2X) frequency in the local cross-flow(inline) direction get amplified while that in the local inline(cross-flow) direction is damped. The 1X frequency components in the local inline direction, represented by the red lines in Figs. 18a-f, have been quickly damped out over a short span of the cylinder. The 2X frequency components in the local cross-flow direction (black lines in Figs. 18g-l), on the other hand, have not diminished, but persist with significant amplitudes until the end of the cylinder.

For all cases, the maximum amplitudes of cross-flow and inline VIVs are found at the end of the cylinder, where significant standing waves are formed as a result of wave reflection. No general trend was observed in the maximum amplitude with respect to the angle α.

5 Motion trajectory and transition of dominant vibrating direction

It has been shown in previous section that two different types of response pattern, one characterized by two opposing travelling waves and the other by a single travelling wave, have been observed in simulations. Two examples of motion trajectories at different locations along the span are presented in Fig. 19 for these two response patterns under flow condition with $\alpha = 45°$. It can be seen from Fig. 19a that the motions of the cylinder with opposing travelling waves are characterized by a figure eight trajectory at most locations along the span, except locations close to the interface between the two flows where the motions exhibit distinct trajectories. These distinct trajectories are caused by the superposition of the two waves that have different vibrating directions and phases. For the response with a single travelling wave, the motion trajectory of the cylinder exhibits regular figure of eight over the whole span, as can be seen from Fig. 19b.

What also can be observed from Fig. 19, and as discussed in the previous section, is a transition of the dominant vibrating direction that occurs at the interface between the two flows. This transition is a result of the change in the direction of cross-flow VIV since its magnitude is significantly larger than that of the inline VIV. Three types of direction transition have been found in simulations. Two of them are observed in the responses with two opposing travelling waves and the other is captured in the responses with single travelling wave. Typical examples of these direction transitions are given in Fig. 20 where the motion trajectories of the cylinder and their dominant vibrating directions at the frequency 1X are plotted. The transition of the dominant vibrating direction in the response with single travelling wave, as shown in Fig. 20c, is quicker and smoother compared to those in the responses with opposing travelling waves as presented in Fig. 20a and b. The transition in single travelling wave takes a direct path from the origin direction to the objective one. However, the change of the direction in opposing travelling waves is not so straight forward. Especially, the transition shown in Fig. 20 takes a long path which first deviates away from the objective direction and then towards it after passes $\theta = 0°$.

The difference in the direction transition patterns as described above can be explained by the fact that the motion of the cylinder in the response with opposing travelling waves is a result of the superposition of the two waves. The vibrating direction of the cylinder is then influenced by the magnitudes of the waves as well as the phase difference between them. This effect is particularly significant at locations (close to interface between the flows) where the two waves just encounter each other and both have equally strong magnitudes,

resulting in different variation patterns in the vibrating direction. It was found that the difference between the two transition patterns observed in responses with opposing travelling waves is mainly due to the phase difference. The two travelling waves that have a phase difference close to π would result in the transition pattern shown in Fig. 20a, while those with a phase difference close to zero would lead to the pattern shown in Fig. 20b.

Nevertheless, the transition of the dominant vibrating direction has been observed in all responses and it normally completes over a short span which is no longer than $0.2L$. Such dramatic change in the vibrating direction could cause significant twist to the cylinder, which should be further investigated with a model considering the coupling between bending and twist.

6 Energy analysis

The energy analysis has been conducted for each steady state response to investigate the energy transfer between the fluid and structure which should provide some insights in the different response patterns discussed in previous sections. The response of the cylinder and the fluid force are fist passed through a band-pass filter and only the motion and force at the dominant frequency 1X and 2X are kept. The energy transfer between the fluid and the structure is then quantified by the work

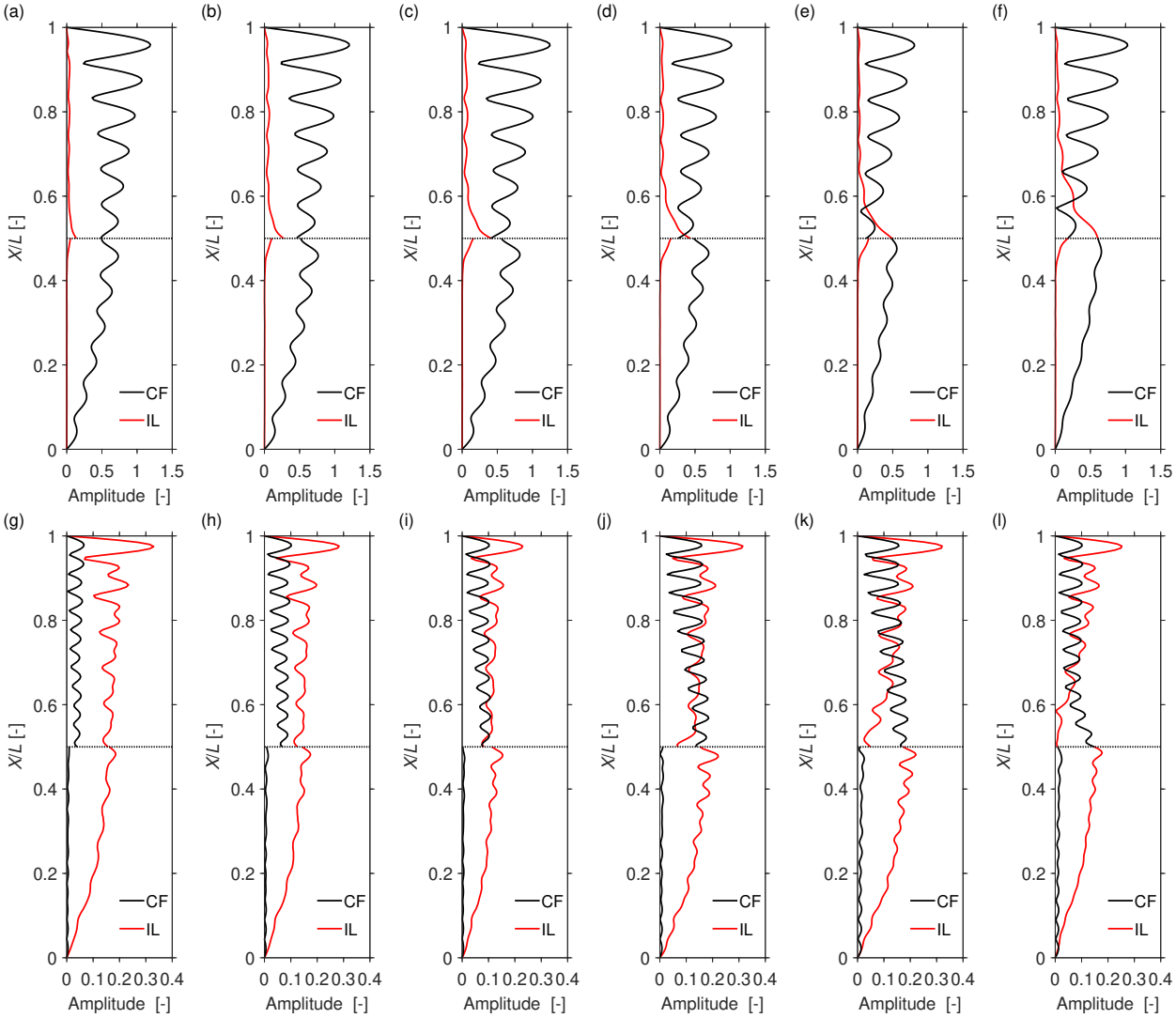

Fig. 18: Normalized amplitudes of displacements at frequencies (a-f) 1X and (g-l) 2X along the cylinder in local cross-flow (CF) and inline (IL) directions for the responses with single travelling wave in flow conditions with (from left to right) $\alpha = 15°$, $30°$, $45°$, $60°$, $75°$ and $90°$. The horizontal dotted line represents the interface between the two flows.

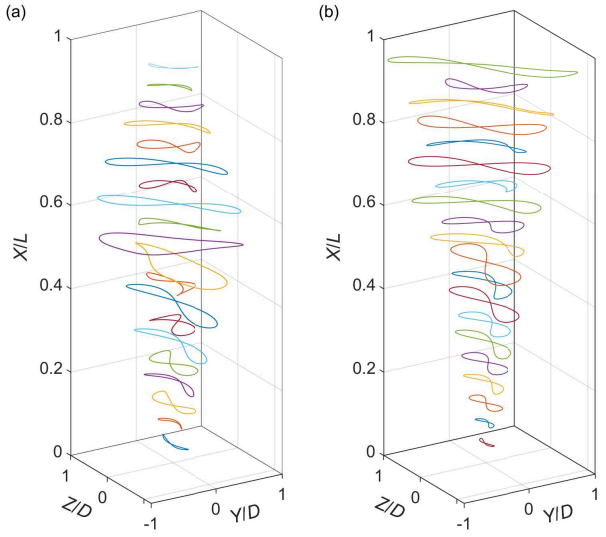

Fig. 19: Motion trajectories of the cylinder at different locations along the span for (a) R1 and (b) R3 responses under the flow condition with $\alpha = 45°$.

done per cycle by the fluid force as

$$W = \int_0^T \mathbf{F}_n \mathbf{v}_n dt \tag{26}$$

where T is the cycle period, $\mathbf{F}_n$ is the nodal force and $\mathbf{v}_n$ is the nodal velocity. In practical implementation, the Eq. (26) is integrated numerically over a time interval that contains at least 50 cycles and the work done per cycle is then achieved by dividing it with the number of cycles.

Same as the displacement, the energy transfer between the cylinder and fluid has been calculated in all vibrating directions. The energy analysis results for the R1 response in the flow condition with $\alpha = 45°$ are presented in Fig. 21. For better illustration, the positive and negative works are distinguished by the warm and cool colors, while no energy transfer is indicated by the white color. It can be seen from Fig. 21a that the cross-flow VIV is subjected to pure excitation by the two flows over the span that away from the interface point. The pure excitation here means that the work done by the fluid is positive, or zero, in all vibrating directions. On the other hand, the energy transfer between the fluid and the structure close to the interface point is characterized by excitations in some directions and damping in others, and the directions of excitation and damping seem to be well separated by the local cross-flow and inline directions.

The excitation and damping directions have been extracted for all R1 responses at $X/L = 0.53$, except that R2 response is taken in the case of $\alpha = 60°$, and results are plotted in Fig. 22. It can be seen from Fig. 22 that the directions of excitation and damping, although not exactly, are well separated by the local cross-flow and inline directions. The directions of damping enclose the cross-flow direction of flow V_1 (dash-dotted line) which approximately represents the vibrating direction of the incoming wave from flow V_1. The distribution of the energy transfer between the fluid and the structure in different directions as shown in Fig. 22 explains the rapid transition of the dominant vibrating direction for the cross-flow VIV. A better illustration is given in Fig. 23, from which it can be seen that the wave of the cross-flow VIV excited by the flow V_1 would be elongated in the direction of excitation and shrink in the direction of damping, resulting in a change of the vibrating direction to comply with the cross-flow of flow V_2.

The directions of maximum excitation and damping that marked in Fig. 22 by diamonds and circles do not represent the best way for vibrating direction transition. The most optimized strategy would be exciting the vibration maximumly in the local cross-flow direction while maximumly damping that in the local inline direction. It can be seen from Fig. 22 that the directions of the maximum excitation and damping gradually move to the best strategy as the angle α between the two flows increases. This implies that at larger angles of α where the transition of the dominant direction becomes more challenging, the hydrodynamic forces acting on the cylinder would tend to seek a better strategy such that a rapid transition is guaranteed.

For the inline VIV, as can be seen from Fig. 21b, the energy transfer between the fluid and the structure shows spanwise alternation of excitation and damping, and such alternation is not observed, or insignificant, with respect to the vibrating direction. This explains why the transition of the dominant vibrating direction is not found in the inline VIV.

To further investigate the cause of such special energy transfer pattern shown in Fig. 22, the motion trajectories of the cylinder corresponding to the 1X frequency are extracted and results are presented in Fig. 24. The locations where the trajectories are extracted are the same as those in Fig. 22. It can be seen from Fig. 24 that all six trajectories have a similar trajectory pattern, with the dominant vibrating direction inclines slightly away from the local cross-flow direction towards the direction of the incoming wave and all trajectories have a counter-clockwise orbital direction.

It is speculated from the above finding that this special energy transfer pattern is related to certain motion trajectories. Therefore, we have generated different motion trajectories by summing two opposing travelling waves with different phase differences ϕ. The local

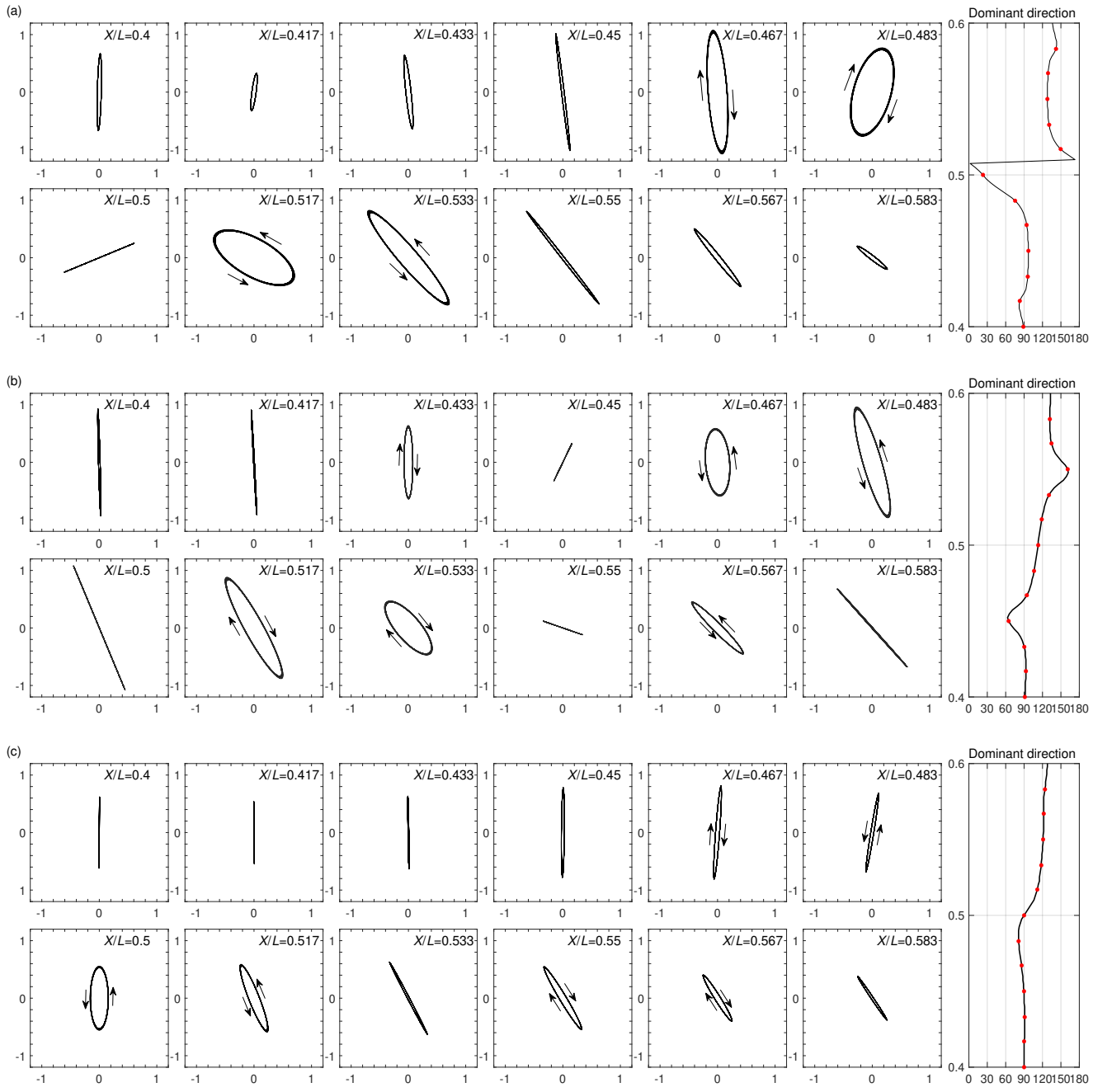

Fig. 20: Motion trajectories and dominant vibrating directions of the cylinder at frequency 1X for the (a) R1, (b) R2 and (c) R3 responses under the flow condition with $\alpha = 45°$. The direction of the local flow is from left to right.

cross-flow direction is set to be parallel with the vibrating direction of one wave (with an amplitude of $0.8D$) and the other wave (with an amplitude of $0.4D$) vibrates in a direction that has a 45° angle with respect to the local cross-flow. A rigid cylinder is forced to vibrate following these prescribed motion trajectories and the forces acting on it are calculated using the hydrodynamic force model described in Section 2. Then, the work done by the fluid force is obtained using Eq. 26. Energy transfer has been calculated for a phase difference varies from 0 to 2π and the results are presented in Fig. 25 together with selected motion trajectories. It can be seen from Fig. 25 that different motion trajectories result in two different energy transfer patterns,

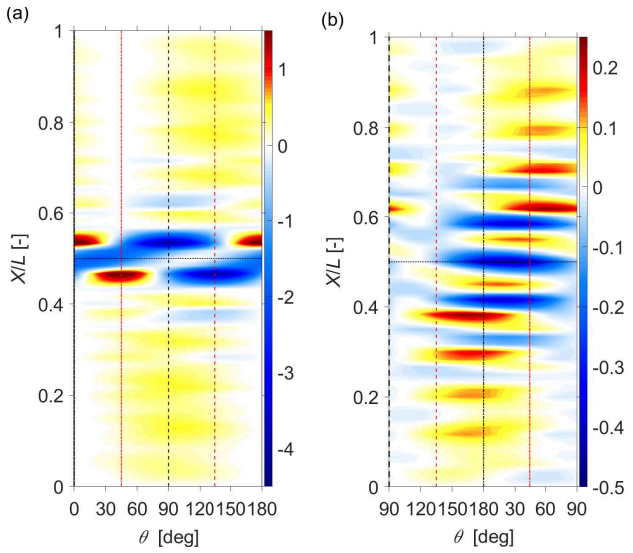

Fig. 21: Energy transfer between fluid and structure at frequencies (a) 1X and (b) 2X for R1 response in the flow condition with $\alpha = 45°$. The horizontal dotted line represents the interface between the flows; vertical black dashed/dash-dotted line represents the cross-flow/inline direction of flow V_1 and vertical red dashed/dash-dotted line represents the cross-flow/inline direction of flow V_2.

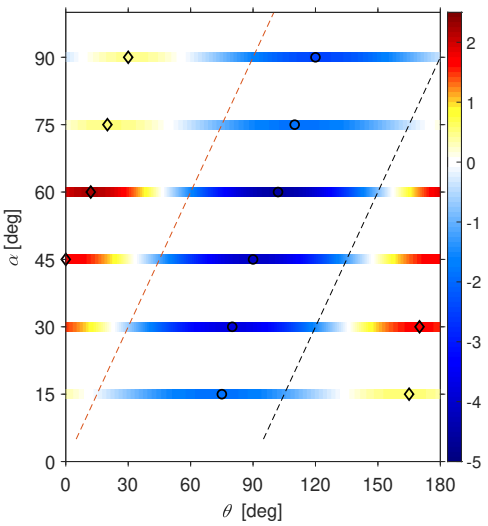

Fig. 22: Energy transfer between fluid and structure at the frequency 1X for R1 responses in flow conditions with $\alpha = 15°$, $30°$, $45°$, $75°$, $90°$ and R2 response in the flow condition with $\alpha = 60°$ at location $X/L = 0.53$. The local cross-flow/inline directions are represented by the black/red dashed lines. The maximum excitation/damping are marked by circles/diamonds.

one in favour of the direction transition and the other against it. The energy transfer that boosts the direction transition is associated with motion trajectories, namely trajectories number 1, 6 7 and 8, that are similar to those shown in Fig. 24. In general, these trajectories have a dominant vibrating direction that deviates away from the local cross-flow direction towards the vibrating direction of the incoming wave (represented by the red dashed lines), and their orbital directions are counter-clockwise. The only exception is the trajectory 1, which has a clockwise orbital direction and may represent a transition from one pattern to the other. It needs to emphasized that the energy transfer calculated here is based on a limited number of motion trajectories generated with two wave amplitudes ($0.4D$ and $0.8D$) and a single difference in the direction ($45°$). A more detailed analysis is required with more combinations of these parameters to reveal the fundamental relations between the energy transfer and motion trajectory.

7 Conclusions

In this paper, VIVs of a flexible cylinder subjected to multi-directional flows have been simulated based on the linear Euler-Bernoulli beam theory and a wake oscillator model. The multi-directional flow refers to

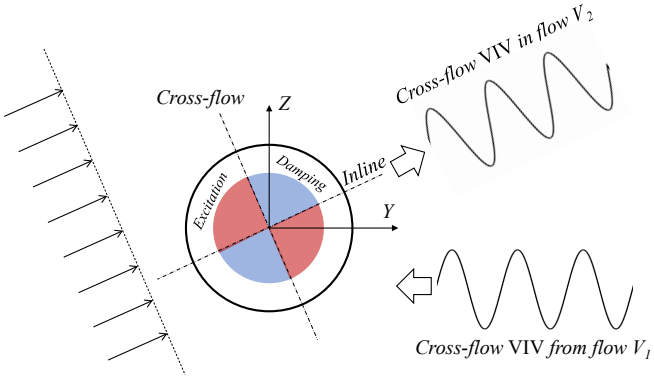

Fig. 23: Illustration of direction transition in cross-flow VIV

a 2-Slab flow with each slab being uniform and unidirectional, and the multi-directional profile is formulated by an angle between the two slabs. Although the model is capable to simulate the VIV of a flexible cylinder subjected to different combinations of flow slabs, the present work focuses on the case where the two slabs are equal in length and velocity, with the angle between the two slabs varying from $15°$ to $90°$.

Different initial conditions have been applied and more than one steady state response has been captured for each flow condition. These steady state responses

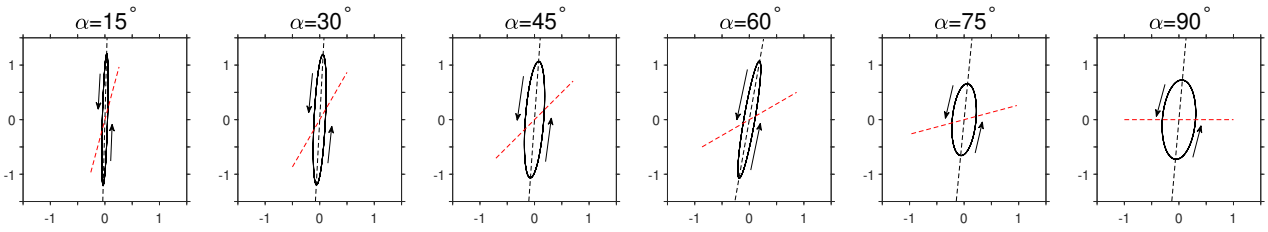

Fig. 24: Motion trajectories at the frequency 1X for R1 responses in flow conditions with α = 15°, 30°, 45°, 75°, 90° and R2 response in the flow condition with $\alpha = 60°$ at location $X/L = 0.53$. The dominant vibrating directions are indicated by black dashed lines and the vibrating directions of incoming waves are indicated by the red dashed lines. The direction of the local flow is from left to right.

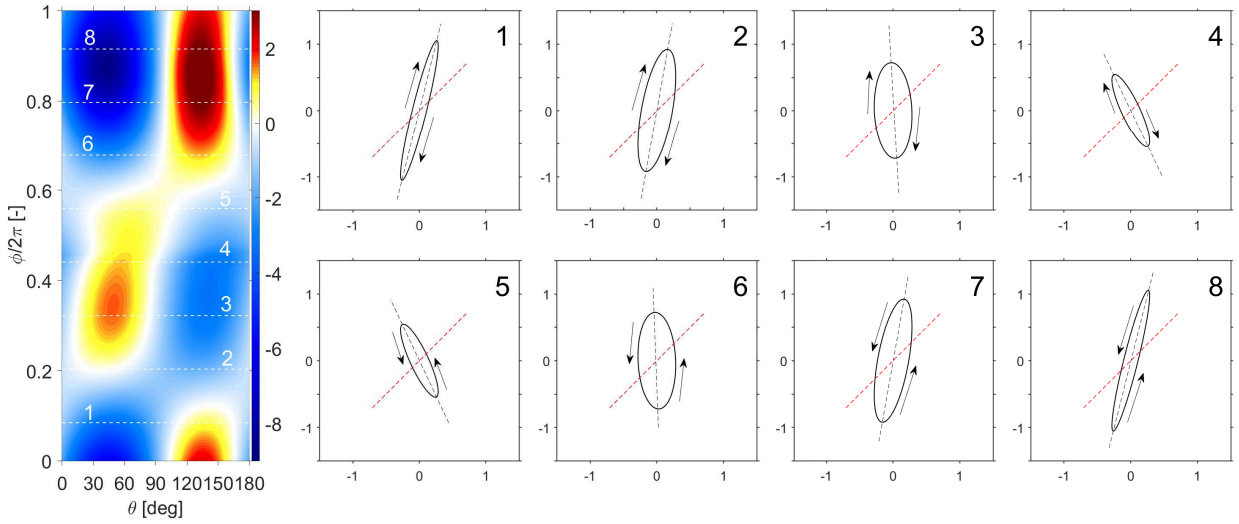

Fig. 25: Energy transfer calculated with prescribed motion trajectories. The local direction of flow is from left to right. The dominant vibrating directions are indicated by black dashed lines and the vibrating directions of the incoming waves (the wave that does not vibrate in the local cross-flow direction) are indicated by the red dashed lines.

can be categorized into two patterns. In one pattern, the response of the flexible cylinder is characterized by two travelling waves that propagate in the opposite directions, while in the other pattern it is dominated by a single travelling wave. For the responses with two opposing travelling waves, it has bee found that even with artificial phase shifts in the initial condition, the simulations would always converge to a few steady state solutions with certain phase differences between the two waves.

In all simulations, a transition of the dominant vibrating direction has been observed to occur close to the interface between the two flows for the cross-flow VIV. Therefore, the cross-flow VIV is found to appear primarily in the local cross-flow direction. However, such transition of the dominant vibrating direction has not been observed in the inline VIV. As a result, vibrations with significant amplitudes at the double frequency (due to inline VIV) have been found in both local cross-flow and inline directions.

Energy analysis has been conducted where the work done by the fluid force per cycle were calculated at each node of the cylinder. It has been shown that the transition of the dominant vibrating direction for the cross-flow is associated to a certain energy transfer pattern between the fluid and the structure. In such energy transfer pattern, the vibration of the cylinder is excited in certain directions while being damped in others, which boosts the vibrating direction of the cross-flow VIV to comply with the local cross-flow direction. Preliminary study on a rigid cylinder with prescribed motions has indicated that such energy transfer pattern is related to certain motion trajectories.

Acknowledgements This work is supported by the National Natural Science Foundation of China (No.52101321,52078010,51825903

Data availability

The datasets generated during and/or analysed during the current study are available from the corresponding author on reasonable request.

Conflict of interest

The authors declare that they have no conflict of interest.

References

1. Bao, Y., Zhu, H., Huan, P., Wang, R., Zhou, D., Han, Z., Palacios, R., Graham, M., Sherwin, S.: Numerical prediction of vortex-induced vibration of flexible riser with thick strip method. Journal of Fluids and Structures **89**, 166–173 (2019). Bluff Body Wakes and Vortex-induced Vibrations (BBVIV-7)
2. Blevins, R.D.: Vortex Induced Vibrations. Van Nostrand Reinhold, New York (1990)
3. Bourguet, R., Karniadakis, G.E., Triantafyllou, M.S.: Distributed lock-in drives broadband vortex-induced vibrations of a long flexible cylinder in shear flow. Journal of Fluid Mechanics **717**, 361–375 (2013)
4. Chen, W., Ji, C., Williams, J., Xu, D., Yang, L., Cui, Y.: Vortex-induced vibrations of three tandem cylinders in laminar cross-flow: Vibration response and galloping mechanism. Journal of Fluids and Structures **78**, 215–238 (2018)
5. Duan, J., Zhou, J., You, Y., Wang, X.: Effect of internal flow on vortex-induced vibration dynamics of a flexible mining riser in external shear current. Marine Structures **80**, 103094 (2021)
6. Facchinetti, M., de Langre, E., Biolley, F.: Coupling of structure and wake oscillators in vortex-induced vibrations. Journal of Fluids and Structures **19**(2), 123–140 (2004)
7. Gao, Y., Pan, G., Meng, S., Liu, L., Jiang, Z., Zhang, Z.: Time-domain prediction of the coupled cross-flow and in-line vortex-induced vibrations of a flexible cylinder using a wake oscillator model. Ocean Engineering **237**, 109631 (2021)
8. Gupta, S.K., Malla, A.L., Barry, O.R.: Nonlinear vibration analysis of vortex-induced vibrations in overhead power lines with nonlinear vibration absorbers. Nonlinear Dynamics **103**, 27–47 (2021)
9. Huera-Huarte, F., Bangash, Z., González, L.: Multi-mode vortex and wake-induced vibrations of a flexible cylinder in tandem arrangement. Journal of Fluids and Structures **66**, 571–588 (2016)
10. Jafari, M., Hou, F., Abdelkefi, A.: Wind-induced vibration of structural cables. Nonlinear Dynamics **100**, 351–421 (2020)
11. Jang, H., Kim, J.W.: Numerical Investigation for Vortex-Induced Vibrations of Steel-Lazy-Wave-Risers: Part II — CFD Study on Long Flexible Riser. In: Proceedings of the ASME 2019 38th International Conference on Ocean, Offshore and Arctic Engineering, vol. Volume 2: CFD and FSI (2019)
12. Kim, S., Kim, S., Kim, H.K.: High-mode vortex-induced vibration of stay cables: monitoring, cause investigation, and mitigation. Journal of Sound and Vibration **524**, 116758 (2022)
13. Kim, S.W., Sævik, S., Wu, J., Leira, B.J.: Time domain simulation of marine riser vortex-induced vibrations in three-dimensional currents. Applied Ocean Research **120**, 103057 (2022)
14. Larsen, C.M., Zhao, Z., Lie, H.: Frequency Components of Vortex Induced Vibrations in Sheared Current. In: Proceedings of the ASME 2012 31st International Conference on Ocean, Offshore and Arctic Engineering, vol. Volume 5: Ocean Engineering; CFD and VIV, pp. 493–501 (2012)
15. Lie, H., Braaten, H., Jhingran, V.G., Sequeiros, O.E., Vandiver, K.: Comprehensive riser viv model tests in uniform and sheared flow. In: Proceedings of the ASME 2012 31st International Conference on Ocean, Offshore and Arctic Engineering, vol. Volume 5: Ocean Engineering; CFD and VIV, pp. 923–930 (2012)
16. Lim, H., Manuel, L., Low, Y.M., Srinil, N.: A surrogate model for estimating uncertainty in marine riser fatigue damage resulting from vortex-induced vibration. Engineering Structures **254**, 113796 (2022)
17. Liu, G., Li, H., Qiu, Z., Leng, D., Li, Z., Li, W.: A mini review of recent progress on vortex-induced vibrations of marine risers. Ocean Engineering **195**, 106704 (2020)
18. Mathis, C., Provansal, M., Boyer, L.: The benard-von karman instability : an experimental study near the threshold. J. Physique Lett. **45**(10), 483–491 (1984)
19. Ogink, R., Metrikine, A.: A wake oscillator with frequency dependent coupling for the modeling of vortex-induced vibration. Journal of Sound and Vibration **329**(26), 5452–5473 (2010)
20. Postnikov, A., Pavlovskaia, E., Wiercigroch, M.: 2dof cfd calibrated wake oscillator model to investigate vortex-induced vibrations. International Journal of Mechanical Sciences **127**, 176–190 (2017). Special Issue from International Conference on Engineering Vibration - ICoEV 2015
21. Qin, L.: Development of reduced-order models for lift and drag on oscillating cylinders with higher-order spectral moments. Ph.D. thesis, Virginia Polytechnic Institute and State University (2004)
22. Qu, Y., Fu, S., Liu, Z., Xu, Y., Sun, J.: Numerical study on the characteristics of vortex-induced vibrations of a small-scale subsea jumper using a wake oscillator model. Ocean Engineering **243**, 110028 (2022)
23. Qu, Y., Metrikine, A.: Modelling of coupled cross-flow and in-line vortex-induced vibrations of flexible cylindrical structures. part ii: on the importance of in-line coupling. Nonlinear Dynamics **103**, 3083–3112 (2021)
24. Qu, Y., Metrikine, A.V.: A single van der pol wake oscillator model for coupled cross-flow and in-line vortex-induced vibrations. Ocean Engineering **196**, 106732 (2020)
25. Sarpkaya, T.: A critical review of the intrinsic nature of vortex-induced vibrations. Journal of Fluids and Structures **19**(4), 389–447 (2004)
26. Song, J., Lu, L., Teng, B., Park, H., Tang, G., Wu, H.: Laboratory tests of vortex-induced vibrations of a long flexible riser pipe subjected to uniform flow. Ocean Engineering **38**(11), 1308–1322 (2011)
27. Song, L., Fu, S., Cao, J., Ma, L., Wu, J.: An investigation into the hydrodynamics of a flexible riser undergoing vortex-induced vibration. Journal of Fluids and Structures **63**, 325–350 (2016)

28. Srivilairit, T., Manuel, L.: Vortex-Induced Vibration and Coincident Current Velocity Profiles for a Deepwater Drilling Riser. Journal of Offshore Mechanics and Arctic Engineering **131**(2) (2009)
29. Trim, A., Braaten, H., Lie, H., Tognarelli, M.: Experimental investigation of vortex-induced vibration of long marine risers. Journal of Fluids and Structures **21**(3), 335–361 (2005). Marine and Aeronautical Fluid-Structure Interactions
30. Violette, R., de Langre, E., Szydlowski, J.: Computation of vortex-induced vibrations of long structures using a wake oscillator model: Comparison with dns and experiments. Computers and Structures **85**(11), 1134 – 1141 (2007). Fourth MIT Conference on Computational Fluid and Solid Mechanics
31. Wang, D., Hao, Z., Pavlovskaia, E., Wiercigroch, M.: Bifurcation analysis of vortex-induced vibration of low-dimensional models of marine risers. Nonlinear Dynamics **106**, 147–167 (2021)
32. Williamson, C., Govardhan, R.: Vortex-induced vibrations. Annual Review of Fluid Mechanics **36**(1), 413–455 (2004)
33. Wu, X., Ge, F., Hong, Y.: A review of recent studies on vortex-induced vibrations of long slender cylinders. Journal of Fluids and Structures **28**, 292–308 (2012)
34. Xu, W., Ma, Y., Ji, C., Sun, C.: Laboratory measurements of vortex-induced vibrations of a yawed flexible cylinder at different yaw angles. Ocean Engineering **154**, 27–42 (2018)
35. Zanganeh, H., Srinil, N.: Three-dimensional viv prediction model for a long flexible cylinder with axial dynamics and mean drag magnifications. Journal of Fluids and Structures **66**, 127 – 146 (2016)
36. Zhang, M., Fu, S., Ren, H., Ma, L., Xu, Y.: A hybrid fem-dnn-based vortex-induced vibration prediction method for flexible pipes under oscillatory flow in the time domain. Ocean Engineering **246**, 110488 (2022)
37. Zheng, H., Wang, J.: A numerical study on the vortex-induced vibration of flexible cylinders covered with differently placed buoyancy modules. Journal of Fluids and Structures **100**, 103174 (2021)
38. Zhu, H., Hu, J., Gao, Y., Zhao, H., Xu, W.: Spatial–temporal mode transition in vortex-induced vibration of catenary flexible riser. Journal of Fluids and Structures **102**, 103234 (2021)